Developmental and Comparative Immunology 109 (2020) 103697

Contents lists available at ScienceDirect

Developmental and Comparative Immunology

journal homepage: www.elsevier.com/locate/devcompimm

Ribosome profiling unveils translational regulation of metabolic enzymes in primary CD4$^+$ Th1 cells

Nicola Manfrini[a,b,1], Sara Ricciardi[a,b,1], Roberta Alfieri[a,2], Gabriele Ventura[b], Piera Calamita[a,b], Andrea Favalli[b], Stefano Biffo[a,b,*]

[a] INGM, National Institute of Molecular Genetics, "Fondazione Romeo ed Enrica Invernizzi", Milano, Italy
[b] Department of Biological Sciences, University of Milan, Milan, Italy

ARTICLE INFO

Keywords:
Ribosome profiling
Th1 cells
Translation
eIF6
eIF4E
mTORC1
PKM2
Metabolism

ABSTRACT

The transition from a naïve to an effector T cell is an essential event that requires metabolic reprogramming. We have recently demonstrated that the rapid metabolic changes that occur following stimulation of naïve T cells require the translation of preexisting mRNAs. Here, we provide evidence that translation regulates the metabolic asset of effector T cells. By performing ribosome profiling in human CD4$^+$ Th1 cells, we show that the metabolism of glucose, fatty acids and pentose phosphates is regulated at the translational level. In Th1 cells, each pathway has at least one enzyme regulated at the translational level and selected enzymes have high translational efficiencies. mRNA expression does not predict protein expression. For instance, PKM2 mRNA is equally present in naïve T and Th1 cells, but the protein is abundant only in Th1. 5′-untranslated regions (UTRs) may partly account for this regulation. Overall we suggest that immunometabolism is controlled by translation.

1. Introduction

Protein synthesis is the decoding of mRNAs into proteins, alias translation. Translational control leads to the selection, starting from the global mRNA pool, of those transcripts requiring to be decoded into proteins (Truitt and Ruggero, 2016). The impact of translation on gene expression has been estimated to be at least as important as transcription (Schwanhausser et al., 2012), meaning that different mRNAs are differentially translated. Translation is divided into four phases: initiation, elongation, termination and recycling. Initiation is the rate-limiting event in the selection of a specific mRNA. At initiation, eIFs (eukaryotic Initiation Factors) perform mechanistic steps under the coordination of signaling pathways (Loreni et al., 2014) and interplay with regulatory elements in the untranslated regions (UTRs) of mRNAs, thus resulting in specific stimulation or inhibition of translation (Hinnebusch et al., 2016). One major pathway controlling initiation of translation is the mTORC1 pathway. mTORC1 stimulates the activity of the eIF4F complex which is necessary for efficient translation of mRNAs containing structured 5' UTRs (Loreni et al., 2014). The relevance of mTORC1 in lymphocyte biology is well established (Zeng and Chi, 2017).

CD4$^+$ T cells are essential for survival (Jung and Paauw, 1998). The transition from naïve T cells to effector T cells requires a complete metabolic rewiring that includes the activation of a glycolytic and fatty acid synthesis program, essential steps for nucleotide biosynthesis and, hence, for cellular growth. It has been traditionally thought that metabolic reprogramming correlates with transcriptional rewiring (Hough et al., 2015). Given the central role of mTORC1 in translation (Loreni et al., 2014), lipid synthesis (Lamming and Sabatini, 2013) and T cell differentiation (Zeng and Chi, 2017), we recently asked whether translational control plays a major role in T cell activation. We found that eukaryotic Initiation Factor 6 (eIF6) is fundamental for the acquisition of effector functions by CD4$^+$ T cells (Manfrini et al., 2017a, 2017b) and that the transition from quiescence to the activated status requires translational control of the lipid biosynthetic pathway (Ricciardi et al., 2018). Overall, these data confirm the hypothesis that translational control is a major player in T cell activation (Piccirillo et al., 2014) and metabolism (Biffo et al., 2018; Brina et al., 2015; Miluzio et al., 2016). Whether translational control of metabolism affects also other stages of T cell differentiation is still unknown.

Abbreviations: Th1 cells, T Helper 1 cells; eIF6, eukaryotic Initiation Factor 6; eIF4E, eukaryotic initiation factor 4E; mTORC1, mammalian target of rapamycin complex 1

* Corresponding author. INGM, National Institute of Molecular Genetics, "Fondazione Romeo ed Enrica Invernizzi", Milano, Italy.
E-mail address: biffo@ingm.org (S. Biffo).

[1] The two authors contributed equally to the work.

[2] Current address: IGM- Institute of Molecular Genetics – CNR, Pavia, Italy.

https://doi.org/10.1016/j.dci.2020.103697
Received 29 January 2020; Received in revised form 6 April 2020; Accepted 6 April 2020
Available online 21 April 2020
0145-305X/

Ribosome profiling is a technology that allows the direct analysis of ribosomal footprints on cellular mRNAs, thus providing a detailed snapshot of translational control (Ingolia et al., 2011). Herein, by using this technique, we investigated the impact of translational regulation on gene expression in $CD4^+$ Th1 cells. Although ribosome profiling has been recently performed in primary mouse T cells (Moore et al., 2018; Myers et al., 2019), our study stands as the first-ever ribosome profiling performed in primary human T cells. Intriguingly, we found that the metabolism of T cells is controlled also at the translational level, confirming that transcriptional studies largely fail in predicting the presence of metabolic enzymes.

2. Materials and methods

2.1. RNA-seq data analysis

RNA-seq data for all human $CD4^+$ T cell subsets were retrieved from (Bonnal et al., 2015) (ArrayExpress E-MTAB-513 experiment). Gene expression levels were estimated by Cufflinks (version 2.0.2) as raw FPKM counts. The heatmap shows z-scored log2-normalized FPKM counts for each gene in different human $CD4^+$ T cell subsets. Heatmaps were generated using Heatmapper (http://www1.heatmapper.ca/expression/). Clustering was performed using the average linkage method and distance measurement was performed using the Pearson method.

2.2. Isolation of human naïve $CD4^+$ T cells and in vitro Th1 differentiation

Blood buffy coats from healthy donors were obtained from Fondazione I.R.C.C.S. Ca' Granda Ospedale Maggiore Policlinico, Milan, Italy. The ethical committee of I.R.C.C.S. Ca' Granda Ospedale Maggiore Policlinico Foundation approved the use of peripheral blood mononuclear (PBMCs) from healthy donors for research purposes and all methods and experiments were carried out in accordance with the Foundation guidelines and regulations. Informed consent was obtained from all subjects in accordance with the Declaration of Helsinki. Human blood primary $CD4^+$ naïve T cells were purified > 95% by negative selection with magnetic beads using the human $CD4^+$ Naïve T cells isolation kit (Miltenyi Biotec, cat # 130-096-533) after previous isolation of PBMCs by Ficoll-paque density gradient centrifugation. Naïve $CD4^+$ T cells were sorted using the following combination of surface markers: $CD4^+$, $CD62L^+$, $CD45RO^-$. Naïve $CD4^+$ T cells were activated *in vitro* with Human T-Activator CD3/CD28 Dynabeads (Life Technologies, cat # 11132D) and IL-2 (20U/ml) and polarized to Th1 by addition of IL-12 (10 ng/ml) and anti-IL-4 (2 μg/ml). Cells were kept 8 days in culture in RPMI medium with 10% FBS, 0.1% Penicillin/Streptomycin (EuroClone), 0.1% nonessential amino acids (Lonza), and 0,1% Sodium Pyruvate (Lonza) at 37 °C and 5% CO_2. At day 6 cells were harvested and the Th1 phenotype was confirmed through FACS analysis by analyzing CXCR3, TBET expression and IFN-γ production.

2.3. Lactate secretion assay and ATP content

After 8 days of Th1 *in vitro* polarization cells were switched to serum-free high-glucose (4,5 g/L) for 4h as indicated in (Brina et al., 2015). Lactate secreted into the medium was measured using a fluorogenic kit (BioVision, cat #K607). Average fluorescence intensities were calculated for each condition replicate. Values were normalized to cell number. For ATP content, $CD4^+$ naïve and 8 days-differentiated Th1 cells were homogenized in 6% (v/v) ice-cold $HClO_4$. Extracts were then centrifuged at 10,000g for 10 min at 4 °C. The acid supernatant was neutralized with K_2CO_3 and used for luminometric determination of ATP (ATP determination kit, Molecular Probes, Thermo Fisher scientific, cat # A22066) using the Lundin method (Lopez-Lluch et al., 2006) as modified in (Calamita et al., 2017).

2.4. Ribosome profiling

After Th1 differentiation, just prior to cell lysis, cells were treated for 2 min with cycloheximide (CHX) 100 μg/ml. Cells were then washed with PBS + CHX 100 μg/ml and lysed in Ribosome Profiling Lysis Buffer (20 mM Tris-HCl (pH7.4), 150 mM NaCl, 5 mM $MgCl_2$, 1 mM DTT, 1% TRITON X-100, 25U/ml Turbo DNase and 100 μg/ml CHX) like in (Ingolia et al., 2011). RNase digestion and monosome isolation were performed as previously described in (Ingolia et al., 2012). Briefly, 11 OD_{254} of total cell lysates (~800 μl) were digested with a total of 4U of RNase I (AM2294; Life Technologies, Carlsbad, CA) for 15 min at 24 °C. Two-hundreds Units of SUPERase-In were then added to stop the digestion. 200 μl of the same lysate was kept as undigested control, and served for input RNA extraction and RNA-seq library preparation. The lysates were then loaded on sucrose cushions (20 mM Tris-HCl (pH7.4), 150 mM NaCl, 5 mM $MgCl_2$, 1 mM DTT, 100 μg/ml CHX, 20 U/ml SUPERase-In plus 1M sucrose) and centrifuged at 70000 rpm for 4 h on a Optima MAX – XP ultracentrifuge (Beckman Coulter) Pellets were then dissolved in 700 μl of Lysis/Binding buffer from the mirVana isolation kit (Thermofisher Scientific AM 1561) and RNA was extracted following kit instructions. Ribosome footprint libraries were prepared according to Ingolia et al. (2012). Purified RNAs were separated on a 15% TBE-Urea acrylamide gel. RNA oligonucleotides of 18 and 34 nucleotides were run alongside with the samples as size markers to cut RNA footprints. After precipitation, size-selected RNAs were depleted of ribosomal RNA using the Ribozero rRNA removal kit (Illumina, cat # MRZH11124) following manufacturer's instructions. RNA fragments were then treated with T4 PNK to remove the 3′ end phosphates. After precipitation, dephosphorylated RNA fragments were ligated to the Universal miRNA cloning linker from New England Biolabs (cat #S1315S). Ligated fragments were then purified through gel electrophoresis on a 15% TBE-Urea gel. After gel extraction, ligated fragments were then reverse transcribed with SuperScript III reverse transcriptase from Life Technologies (cat # 18080-044) and the following reverse transcription primer: 5′-(Phos)-AGATCGGAAGAGCGTCGTGTAGGGAAAGAGTGTAGATCTCGGTGGTCGC-(SpC18)CACTCA-(SpC18)-TTCAGACGTGTGCTCTTCCGATCTATTGATGGTGCCTACAG). Reverse transcription products were gel-purified and precipitated. After precipitation, cDNAs were circularized using the CircLigase from Epicentre (cat # CL4111K). Following circularization, cDNAs were precipitated and used to set up pilot PCR reactions. PCR reactions were prepared using the Phusion HF buffer, 2 mM dNTPs, 0.5 μM of the Forward library PCR primer (5′-AATGATACGGCGACCACCGAGATCTACAC-3′), 0.2 mM reverse indexing primers, 5 μl of eluate template, 2 U of Phusion polymerase (cat #M0530L; NEB). Amplification was examined by gel electrophoresis on an 8% TBE polyacrylamide gel. Once optimal cycles for each library were determined, additional PCR reactions were performed and run on an 8% TBE polyacrylamide gel. The products were then cut out and DNA extracted from the gel slice and quality control performed on a 2100 Agilent bioanalyzer using Agilent's DNA high sensitivity kit (5067-4626). One single library was prepared from the pooling of three independent biological replicates.

2.5. RNA-seq library preparation and high-throughput sequencing

RNA-seq samples were prepared using the Illumina TruSeq Stranded Total RNA Library Prep Kit (20020596) according to manufacturer's instructions. Three independent libraries were prepared from three independent biological replicates. Library sequencing for both Ribo-seq and RNa-seq samples was performed using the Rapid Run SR100 mode on Illumina HiSeq2000. Samples were sequenced by the NGS Facility (LABSSAH) at the Centre for Integrative Biology (CIBIO), University of Trento. Raw sequence data are available at ArrayExpress, accession number E-MTAB-5961.

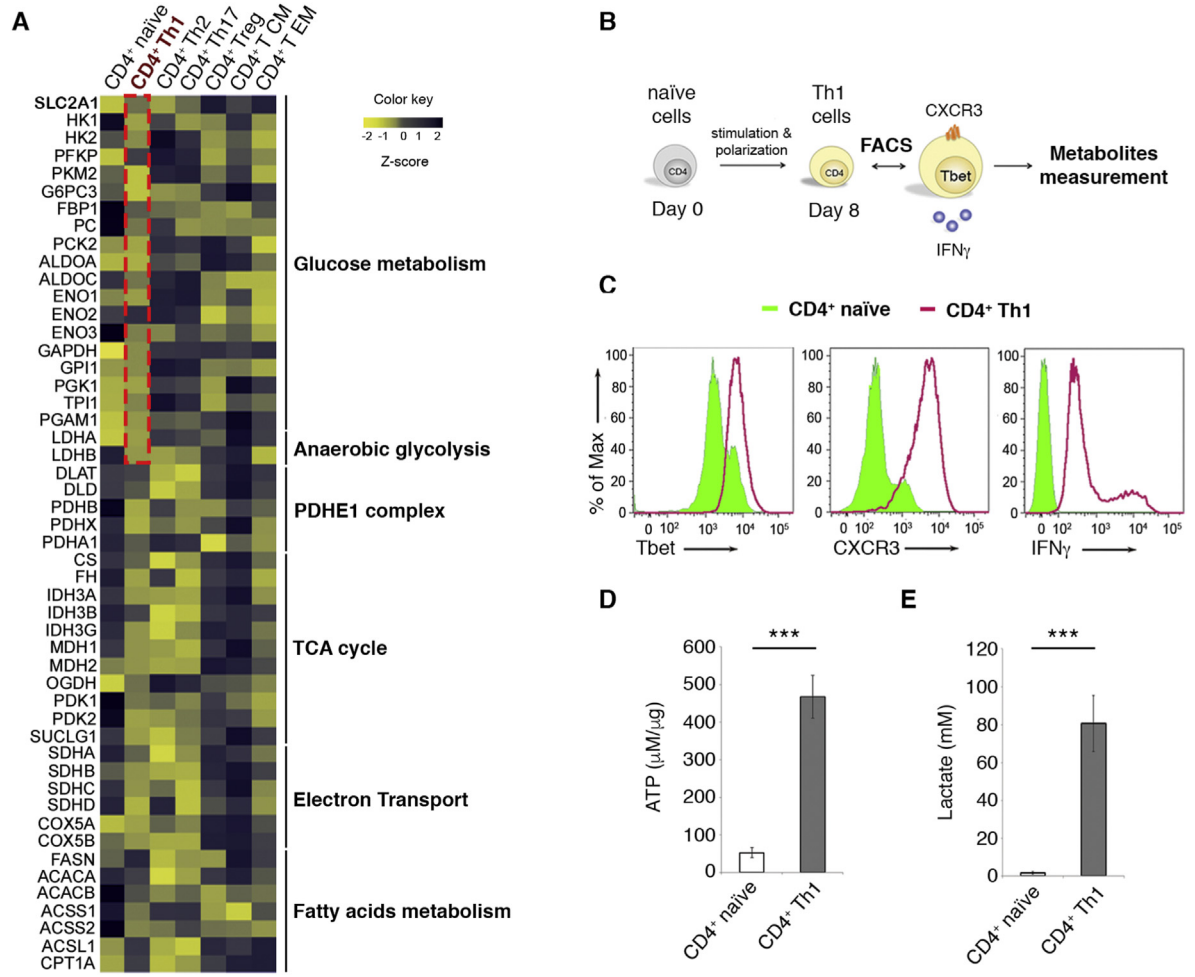

Fig. 1. Th1$^+$ cells have high lactate secretion (glycolysis) and low mRNA levels of glycolytic enzymes.
(A) Heatmap representing mRNA levels of metabolic enzymes in different CD4$^+$ T cell subsets. Enzymes were grouped in metabolic pathways as previously described and clustered (Ricciardi et al., 2018). Th1$^+$ cells have lower amounts of glycolytic mRNAs when compared to naïve T cells. (B) Experimental outline of Th1 differentiation. Human naïve CD4$^+$ T cells were isolated from the blood of three healthy donors and *in vitro* polarized to Th1 for 8 days. (C) FACS analysis of Th1 specific markers. After polarization to Th1 (see Fig. 1B), the Th1 cellular phenotype was confirmed by FACS through analysis of the expression of transcriptional factor Tbet, of surface marker CXCR3 and through IFN-γ intracellular staining. (D-E) ATP (D) and lactate (E) levels in naïve, and in Th1 cells. Data are representative of three independent experiments (n = 3). Error bars represent Standard Deviation. Statistical *p*-values were calculated using the two-tailed *t*-test (NS: *p*-value > 0.05; ***: *p*-value < 0.001).

2.6. Reads preprocessing and alignments

Raw reads were checked for quality by FastQC software (version 0.11.2), then cleaned of 3' custom adapters, filtered by quality scores and length using Trimmomatic (version 0.32). Only the reads with a quality score greater than 3 and longer than 24bp were maintained. The trimmed reads were aligned to human rRNA sequences (5S, 5.8S, 18S and 28S) using Bowtie 2, version 2.2.5. The reads uniquely aligned to rRNA were discarded from the samples. The remaining reads were mapped to human reference genome assembly GRCh38 (Ensembl release 83) with STAR aligner (version 2.5.0b). Read alignments were assigned to genomic coordinates using SAMtools (version 1.2), by sorting and indexing the *bam* files generated by STAR. Genomic tracks for ribosome profiling and RNA-seq samples were visualized using IGV software and compared to other published Ribo-seq experiments through the GWIPS-viz web tool (Michel et al., 2015).The RNA-seq reads were analyzed using the same steps as the ribosome profiling reads.

2.7. Quality assessment of ribosome profiling data

The quality control of the ribosome sequencing in terms of reads lengths was verified using the *RiboProfiling* library in R environment. The sizes of reads corresponding to ribosome footprints (expected around 30bp) were calculated and plotted in a histogram starting from a *GAlignment* object (the loaded records of the BAM file). The countShiftReads function quantified the coverage on different sequence features thus it was used to count reads on particular genomic features (e.g. 5pUTR, CDS, 3pUTR). The countsPlot function generated a boxplot of counts divided by 5′UTR, CDS, 3′UTR regions.

2.8. Measurements of gene expression and isoforms quantification

The quantification of expression at the gene level was measured by STAR through the option "quantMode GeneCounts" using the annotation GTF file from the Ensembl release 83. STAR allows to count the number of reads per gene while mapping. For the quantitative analyses, only uniquely mapped reads were considered. A read was counted if it overlaps exclusively one gene. The counts for unstranded RNA-seq were selected. Read counts for ribosome profiling and RNA-seq were

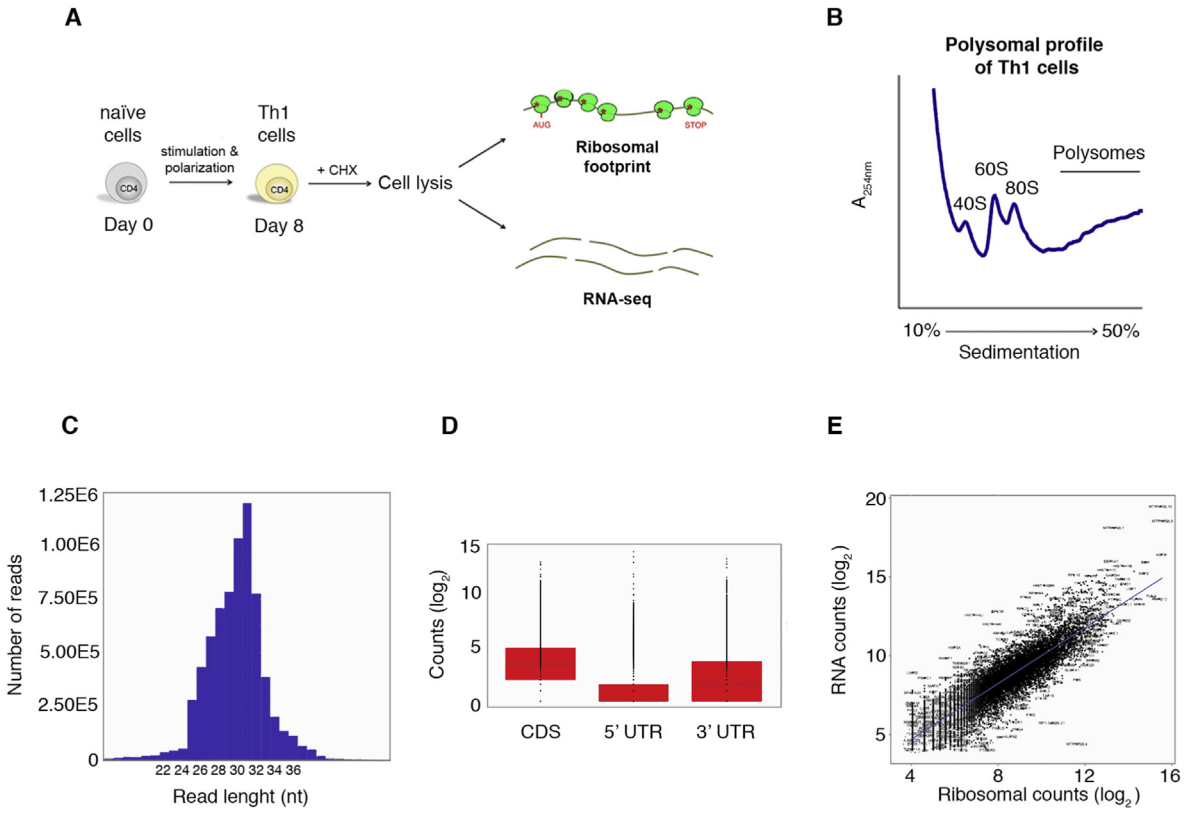

Fig. 2. Ribosome profiling of *in vitro* differentiated human CD4$^+$ T_h1 cells.
(A) Ribosome profiling strategy for *in vitro* differentiated CD4$^+$ Th1 cells. After 8 days of T_h1 *in vitro* polarization cells were lysed and ribosomal footprinting was performed. (B) Polysome profile of Th1 cells, *in vitro*, before ribosome profiling. (C) Read length distribution for ribosome profiling reads centers at 30 nucleotides. (D) Coverage of footprint reads on different genomic sequence features. (E) Scatter plot representing RNA counts vs ribosomal counts of total genes. Total RNA-seq read counts were plotted against Ribosomal-seq reads obtained from the same samples *in vitro* differentiated to T_h1 for 8 days.

normalized in the R environment according to the *size factor* estimated by DESeq2 library using the median-of-ratios method to account for differences in sequencing depth between samples. The quantification of isoforms expression level was estimated using the RSEM software (version 1.2.15) using the Ensembl Release 83 as reference genome. Genes with < 10 RFP reads and/or < 20 RNA reads were excluded.

2.9. GO analysis

GO analysis was performed on the top 1000 genes enriched in ribosomal counts and on the top 1000 genes depleted for ribosomal counts using "Generic Gene Ontology (GO) term finder" (https://go.princeton.edu/cgi-bin/GOTermFinder).

The same tool was used on the top 20 genes with the highest TEs, on the top 20 genes with the lowest TEs, and on the full lists of gene with significantly high or low TEs.

2.10. Translational efficiency calculation

Translational efficiency (TE) for protein coding genes was calculated as the $\log_2$ ratio of footprint-normalized counts to the average of mRNA-normalized counts.

A positive TE value means that ribosomal counts are relatively more enriched than RNA counts, which suggests a high translational rate for the specific gene analyzed. A negative TE value means that ribosomal counts are relatively less enriched that RNA counts suggesting a low translational rate for the specific gene analyzed. Genes with normalized raw RNA reads < 100 were excluded from the analysis.

The global translational efficiency (global TE) index for each pathway was calculated as the mean of all the TEs of genes involved in that specific pathway.

2.11. Visualization of RNA-seq and ribo-seq tracks

RNA-seq and ribo-seq tracks of the genes of interest were visualized with Integrated Genome Viewer (IGV), version 2.6.2, using the autoscale method for visualization of reads.

2.12. Secondary structure analysis of 5' UTR regions

5' UTR secondary structure predictions were calculated using the "Predict a secondary structure" web server using the RNAStructure software tool (https://rna.urmc.rochester.edu/RNAstructureWeb/Servers/Predict1/Predict1.html).

2.13. Polysomal profiles

Polysomal profiling was performed as previously described (Gallo et al., 2018; Gandin et al., 2010). In brief, cells were lysed in 30 mM Tris-HCl, pH 7.5, 100 mM NaCl, 30 mM $MgCl_2$, 0.1% NP-40, 10 mg/ml cycloheximide and 30 U/ml RNasin. Cytoplasmic extracts with equal amounts of RNA were loaded on a 15–50% sucrose gradient and centrifuged at 4 °C in a SW41Ti Beckman rotor at 39,000 rpm. Absorbance at 254 nm was recorded using the BioLogic LP software (BioRad) and 8 fractions (1 ml each) were collected for subsequent RNA extraction.

2.14. Analysis of translated mRNAs

mRNAs collected from the fractions of sucrose gradients, were divided, during polysome profiling analysis, into subpolysomal and

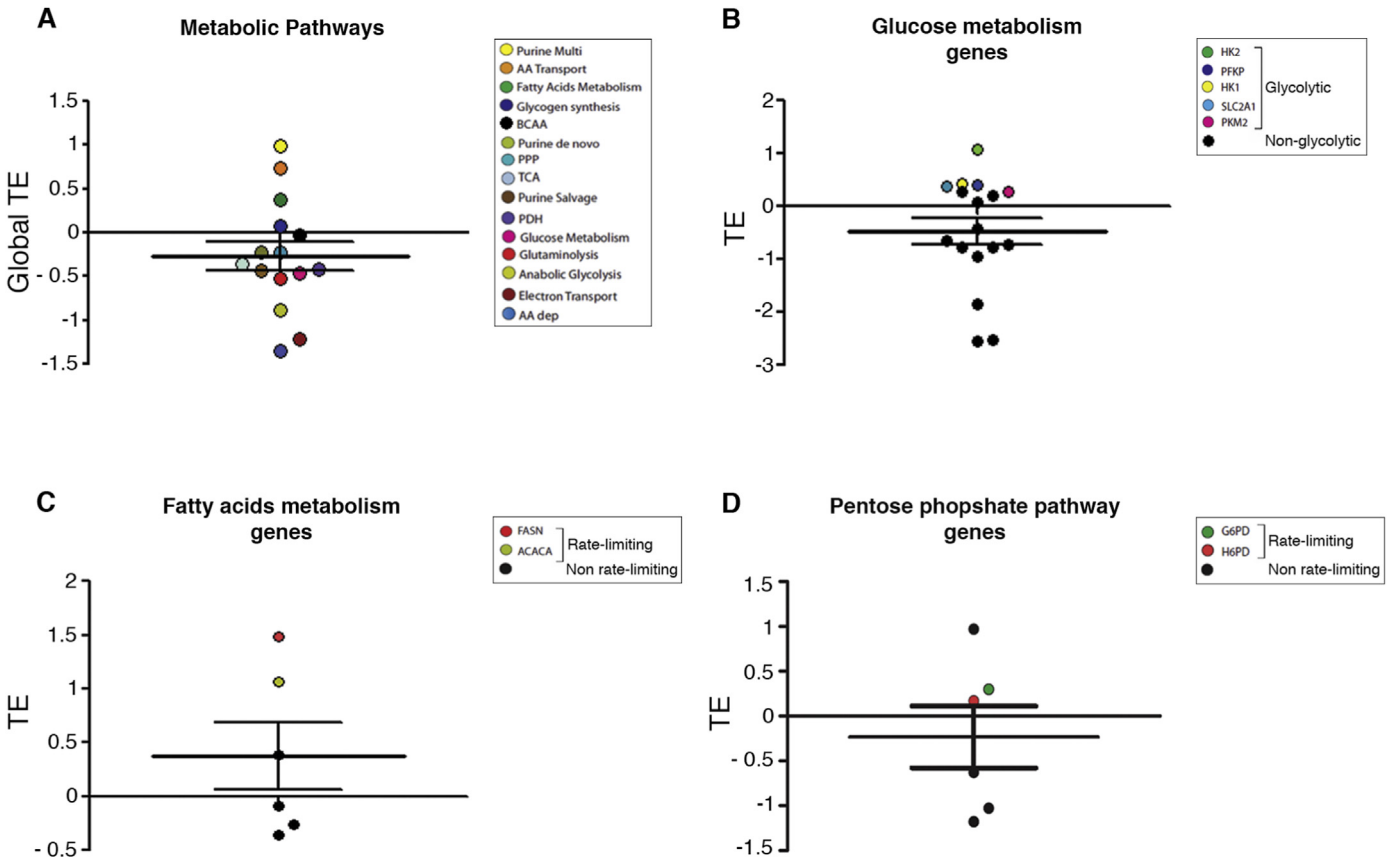

Fig. 3. Translational efficiencies (TE) vary among different pathways and between different enzymes within the same pathway.
(A) Scatter dot plot representing mean metabolic pathway TEs. Each pathway is represented by a dot and each color represents a different metabolic pathway (See color legend). (B) Scatter dot plot of genes involved in Glucose metabolism. Each gene is represented by a dot. Genes involved in irreversible steps of glycolysis are colored (See color legend). (C) Scatter dot plot of genes involved in Fatty Acids Metabolism. Each gene is represented by a dot. Fatty Acid Synthesis genes encoding for enzymes involved in irreversible reactions are colored in red and yellow (See color legend). (D) Scatter dot plot of genes involved in the PPP. Each gene is represented by a dot. PPP genes encoding for enzymes involved in irreversible reactions are colored in red and green (See color legend). Horizontal lines represent mean values while error bars represent SEMs. TE: translational efficiency. . (For interpretation of the references to color in this figure legend, the reader is referred to the Web version of this article.)

polysomal fractions. Samples were then incubated with proteinase K and 1% SDS for 1 h at 37 °C. RNAs were then extracted using the phenol/chloroform/isoamyl alcohol method.

2.15. Total RNA extraction

Total RNAs were extracted using the RNeasy kit (Qiagen, cat # 74104) following manufacturer's instructions.

2.16. Reverse transcription for RT-qPCR

Reverse transcription was performed using SuperScript III First-Strand Synthesis System (Thermo Fisher Scientific, cat # 18080051) following manufacturer's instructions.

2.17. mRNA extraction for real-time RT–qPCR

RT-qPCR reactions were performed using the GoTaq qPCR Master Mix (Promega cat # A6001) as previously described (Ricciardi et al., 2018) and the following oligos: HK1: Fwd: 5′ TCCGTAGTGGGAAAAA GAGAA3'; Rev: 5′ GACAATGTGATCAAACAGCTC3'; PKM2: Fwd: 5′ GGCTGAGAATACTGCCACACT3'; Rev: 5′ACCGTCTTGCTCTCTACT CGT3'; FASN: Fwd: 5'GATGACCGTCGCTGGAAG'3; Rev: 5′CTGAGGGT CCATCGTGTGT3'; TPI1: Fwd: 5′CTCATCGGCACTCTGAACG3'; Rev: 5′ GCGAAGTCGATATAGGCAGTAGG3'; G6PD: Fwd: 5′ACCGCATCGACC ACTACCT3'; Rev: 5′TGGGGCCGAAGATCCTGTT3'; RPS29: Fwd: 5′TCT CGCTCTTGTCGTGTCTG3'; Rev: 5′CCGATATCCTTCGCGTACTG3'; β-ACTIN: Fwd: 5′AGAGCTACGAGCTGCCTGAC3'; Rev: 5′CGTGGATGCC ACAGGACT3'. β-ACTIN was used as internal standard. All reactions were performed on StepOnePlus Real-Time PCR Systems (Thermo Fisher Scientific). Data are expressed as mRNA levels normalized over β-actin. Results are represented as means ± standard deviation of three independent experiments.

For RT-qPCR on mRNAs derived from polysome fractions, mRNA abundance in each of the fractions was quantitated as the percentage over the total mRNA.

2.18. Western blotting and antibodies

SDS-PAGE was performed on protein extracts obtained from human $CD4^+$ naïve T cell or from $CD4^+$ T cells *in vitro* differentiated to Th1 as previously described. Western blotting was performed as previously described (Ricciardi et al., 2018). The following antibodies were used for western blotting: PKM1/2 antibody (Cells Signaling, cat # 3186) and TPI antibody (Santa Cruz, cat # 22031). Chemiluminescent signals were detected using Amersham ECL Prime (GE Healthcare Life Sciences, ct # RPN2232) and images were acquired using the LAS-3000 imaging system from Fuji.

2.19. Immunofluorescence

Immunofluorescence was performed as previously described

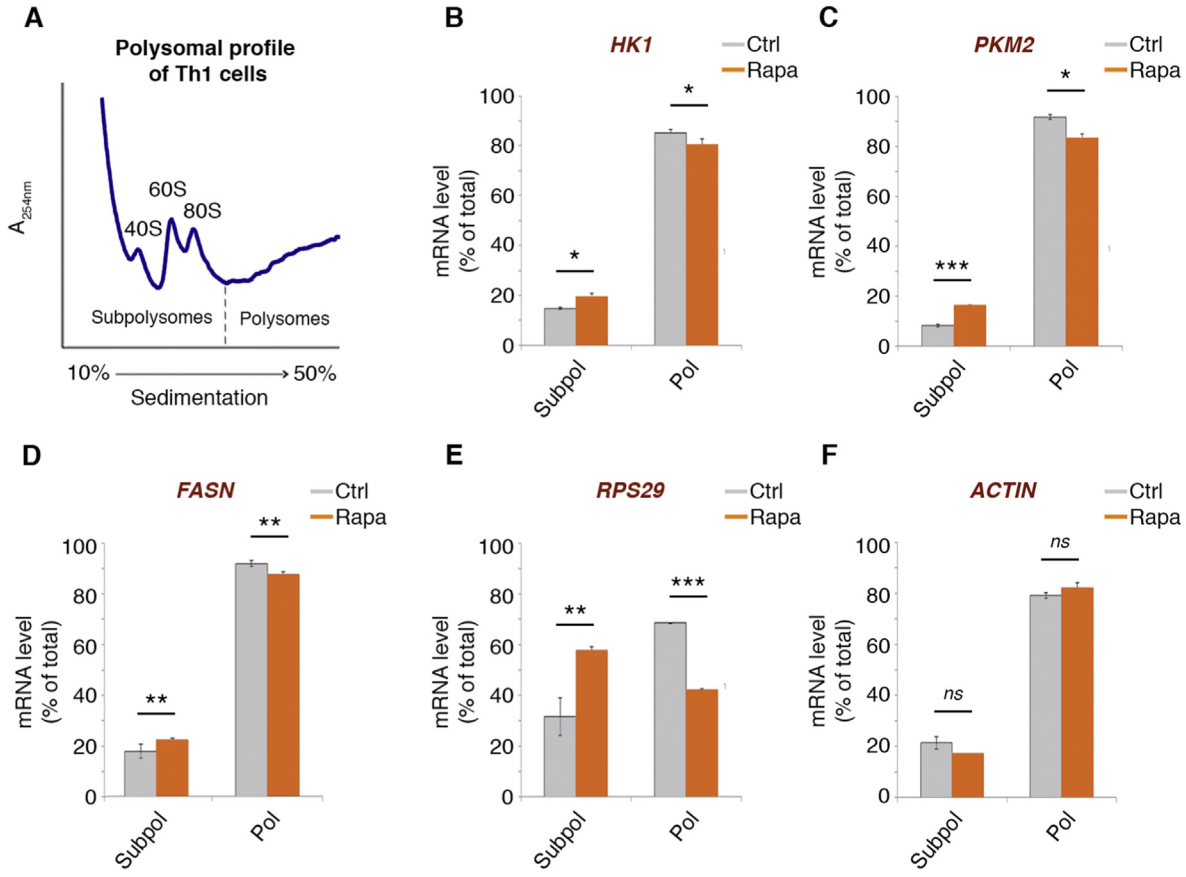

Fig. 4. Polysomal association of genes regulated at the translational level confirms data on translational efficiency and indicates differential sensitivity to mTORC1 inhibition.
(A) Naïve CD4$^+$ T cells were isolated from PBMCs of healthy donors and kept untreated or polarized *in vitro* to Th1 for 8 Days. Polysomal profile of *in vitro* polarized Th1 cells. (B-F) Quantification of mRNA levels of HK1, PKM2, FASN, RPS29 and β-Actin in polysomal and subpolysomal fractions of naïve CD4$^+$ T cells isolated from PBMCs of healthy donors and polarized *in vitro* to Th1 for 8 days. Cells were left untreated (Control) or treated for 4 h with 100 nM Rapamycin. RPS29 is a rapamycin sensitive mRNA, whereas β-Actin is not rapamycin sensitive. HK1, PKM2 and FASN association with polysomes is very robust, in line with ribosome profiling data, but partly sensitive to rapamycin, suggesting regulation by multiple pathways. Error bars represent Standard Deviation. Statistical *p*-values were calculated using two-tailed *t*-tests (NS: *p*-value > 0.05; *: *p*-value < 0.05; **: p-value < 0.01; ***: *p*-value < 0.001), n = 3.

(Gandin et al., 2008). Primary antibodies were used at the following dilutions: rabbit PKM1/2 (1:100; Cell Signaling). Alexa Fluor 488-conjugated secondary antibody (Thermo Fisher Scientific) was added for 2h at room temperature. Slides were mounted in Mowiol 4–88 mounting medium (Sigma-Aldrich). Fluorescence images were acquired using a confocal microscope (Leica TCS SP5) at 1,024 Å~ 1,024 dpi resolution. All the images were further processed with Photoshop CS6 (Adobe) software.

2.20. FACS analysis

FACS analysis was performed as previously described (Manfrini et al., 2017b). For Th1 phenotyping 500000 cells per sample were stained with the following antibodies: V450 mouse anti-human IFN-γ (BD Biosciences, cat # 560371), PE mouse anti-human CD183 (CXCR3) (BD Pharmingen, cat # 557185), Anti-human T-bet eFluor 660 (Thermo Fisher Scientific, cat # 50-5825-82). PKM2 staining was performed on 1 million cells/sample using anti-PKM1/2 (Cell Signaling, cat # 3186) as primary antibody and Alexa Fluor 448 goat anti-rabbit (Invitrogen, cat # A11008) as secondary antibody.

2.21. Statistical analysis

Unless otherwise stated, all results were analyzed using coupled two-tailed *t*-tests. Where indicated unpaired single-tailed *t*-tests were used. A *p*-value of < 0.05 was considered significant (*: $p < 0.05$; **: $p < 0.01$; ***: $p < 0.001$; NS: not significant).

3. Results

3.1. Translational control regulates entire metabolic pathways

We have recently demonstrated that translation regulates the metabolic shift required for activating quiescent naïve CD4$^+$ T cells (Ricciardi et al., 2018). We asked whether translational control played also a role in controlling the metabolism of effector CD4$^+$ T cells. We investigated a previously published RNAseq dataset from 7 different human CD4$^+$ T cell subsets (Bonnal et al., 2015), in order to highlight transcriptional profiles that might suggest a layer of translational regulation. We found that, among all effector T cell subsets, Th1 cells presented the lowest levels of mRNAs encoding for enzymes involved in glucose metabolism and anaerobic glycolysis (Fig. 1A). Since Th1 cells are known to depend on glycolysis (Peng et al., 2016), this suggested the presence of a layer of post-transcriptional regulation to increase their glycolytic potential. Therefore, we analyzed terminally differentiated Th1 cells. We polarized *in-vitro* human CD4$^+$ naïve T cells to Th1 (Fig. 1B). After 7 days of differentiation, most cells expressed all Th1-specific markers (Fig. 1C, left and center) including the Th1-specific cytokine IFN-γ (Fig. 1C, right). Compared to naïve T cells, differentiated Th1 lymphocytes presented high ATP (Fig. 1D) and lactate

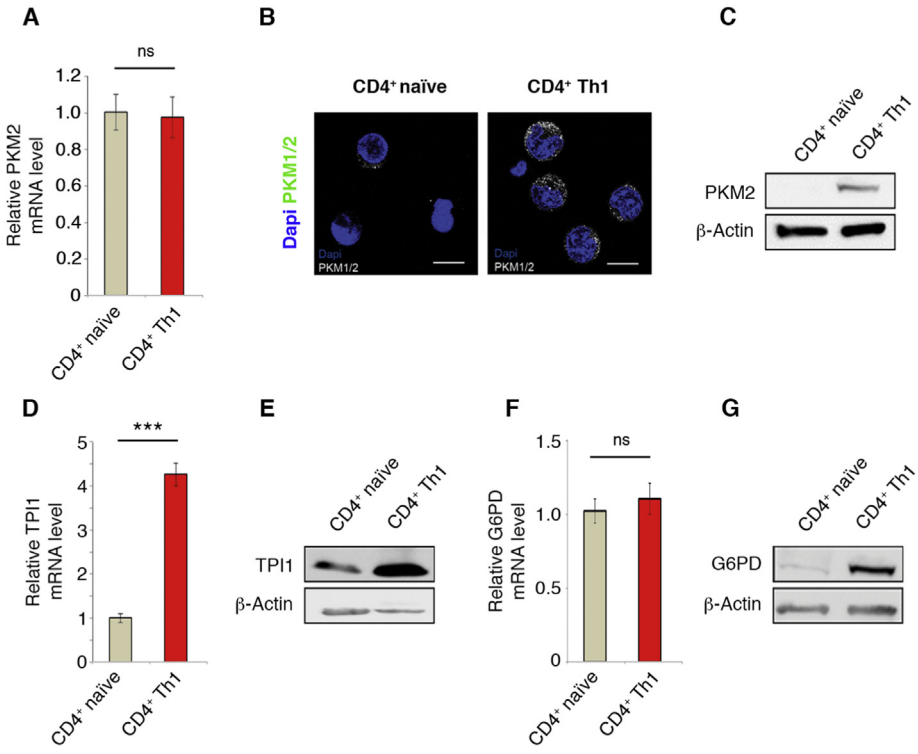

Fig. 5. Lack of correlation between mRNA and protein levels demonstrates the relevance of translational efficiency in gene expression.
(A-C) Gene expression of PKM2. For both CD4$^+$ naïve T cells left untreated or polarized *in vitro* to Th1, PKM2 RNA and protein levels were assessed. (A) PKM2 mRNA levels of Th1 cells were normalized to β-actin and plotted in percentage to expression levels in naïve CD4$^+$ T cells. (B) Imunofluorescence detection of PKM2. A Double-immunostaining for nuclei (DAPI) and for PKM2 was performed. Scale bars: 10 μm. (C) Representative Western Blot of PKM2 protein in CD4$^+$ naïve T cells and Th1. Data demonstrate that PKM2 protein expression is not associated with mRNA levels, but depends on its high TE. (D-E) Gene expression of TPI1. For both CD4$^+$ naïve T cells left untreated or polarized *in vitro* to Th1, TPI1 RNA and protein levels were assessed by RT-qPCR (D) and western blotting (E). Target mRNA levels were normalized to β-actin and are relative to expression levels in naïve CD4$^+$ T cells. Data demonstrate that TPI1 protein levels largely correlate with mRNA expression. (F-G) Gene expression of G6PD. Experiments performed as described for (D-E). Data demonstrate that G6PD protein levels only partly correlate with mRNA expression. All data are representative of three independent experiments (n = 3). Error bars represent Standard Deviation. Statistical *p*-values were calculated using the two-tailed *t*-test (NS: *p*-value > 0.05; ***: *p*-value < 0.001).

levels (Fig. 1E, right), features which are in line with an active glycolytic program but could not be predicted by transcript abundance.

We hypothesized that translation might play a role in regulating the metabolism of Th1 cells. To validate our hypothesis, we performed ribosome profiling in human CD4$^+$ Th1 cells diffentiated *in vitro* (Fig. 1B; 2A). Polysomal profiles showed that the Th1$^+$ population was translationally active *in vitro*, as shown by the high polysome/80S ratio (Fig. 2B). After proper RNAse digestion of polysomes, the samples were used for preparation of ribosome profiling (ribo-seq) and total RNA libraries (Supplementary File 1). Ribo-seq libraries presented a length distribution of approximately 28–30 nts, as expected for ribosome-protected reads (Fig. 2C) and good coverage of coding sequences (Fig. 2D). At first, we analyzed the distribution of RNA counts over ribosome counts. Although most transcripts fell in the confidence region, several genes showed significant enrichment or decrease of ribosomal counts (Fig. 2E), suggesting that differential translation may act as a driving force in regulating gene expression in Th1 cells. Such genes were mostly involved in cell signaling, differentiation and development or in anabolic/catabolic cellular processes (Supplementary File 1; ArrayExpress, accession number E-MTAB-5961).

To evaluate more precisely the impact of translation in regulating gene expression, we calculated the translational efficiency (TE) of each gene detected by our RNA-seq analysis, namely the $\log_2$ ratio of footprint-normalized counts over the average of mRNA-normalized counts (Supplementary File 1). The rationale of our TE calculation is to define, among the total pool of mRNAs, those specific transcripts which are preferentially translated in our cellular setup. By these means we found that the top 20 genes with the highest TEs were involved in RNA splicing and processing while the top 20 genes with lowest TEs were involved in nucleosome organization and chromatin assembly (Supplementary File 1). When we analyzed all those genes whose TE was significantly higher or lower than the mean, we found mainly genes involved in metabolic pathways, confirming the notion that translation can act as a master regulator of cellular metabolism. Next, we focused on metabolic genes. In order to understand to which extent the activation of a specific metabolic pathway depended on translation, we introduced the global TE index that can be defined roughly as the mean of the TEs of all the genes acting in the same pathway. We show that the global TE index widely varies in different pathways (Fig. 3A). We found that pathways involved in amino acid transport and purine synthesis showed the highest global TEs, while the electron transport and amino acid deprivation pathways had the lowest global TEs (Fig. 3A). Summarizing, our data suggest that in human Th1$^+$ cells translation contributes to the control of entire metabolic pathways.

3.2. Translational control discriminates between reversible and irreversible reactions and accounts for specific protein expression in the presence of equal amounts of mRNA

Several metabolic pathways fell in the median-value region, i.e. presented average global TEs (Fig. 3A). Next, we analyzed the TE of single genes belonging to the same pathway. Notably, we found that within pathways with average TEs, some genes showed higher TE. The first example relates to gluconeogenesis. Gluconeogenesis is the synthesis of glucose from pyruvate, roughly the reverse of glycolysis. Some enzymes are shared by both glycolysis and gluconeogenesis, because they perform reversible reactions, whereas some virtually perform irreversible reaction. In general, we found that common glycolysis/gluconeogenesis enzymes had abundant mRNAs but no translational enrichment, and low TEs, (Fig. 3B; Supplementary File 1), suggesting their expression being switched on primarily at the transcriptional level, exception made for GPI1, the only enzyme to show a positive TE among all common glycolysis/gluconeogenesis genes (Supplementary File 1). Rate limiting gluconeogenesis-specific enzymes had reduced TEs and/or low or undetectable mRNAs (Supplementary File 1), thus suggesting that gluconeogenesis, a pathway known to be inactive in effector T cells, is predominantly switched off at the transcriptional level. In contrast, glycolytic enzymes, which *per se* control catabolic irreversible reactions, presented the highest TEs within the glucose metabolism pathway, e.g. HK2 (Fig. 3B), suggesting their expression being translationally regulated.

Concerning the fatty acid synthesis pathway, we found that rate-

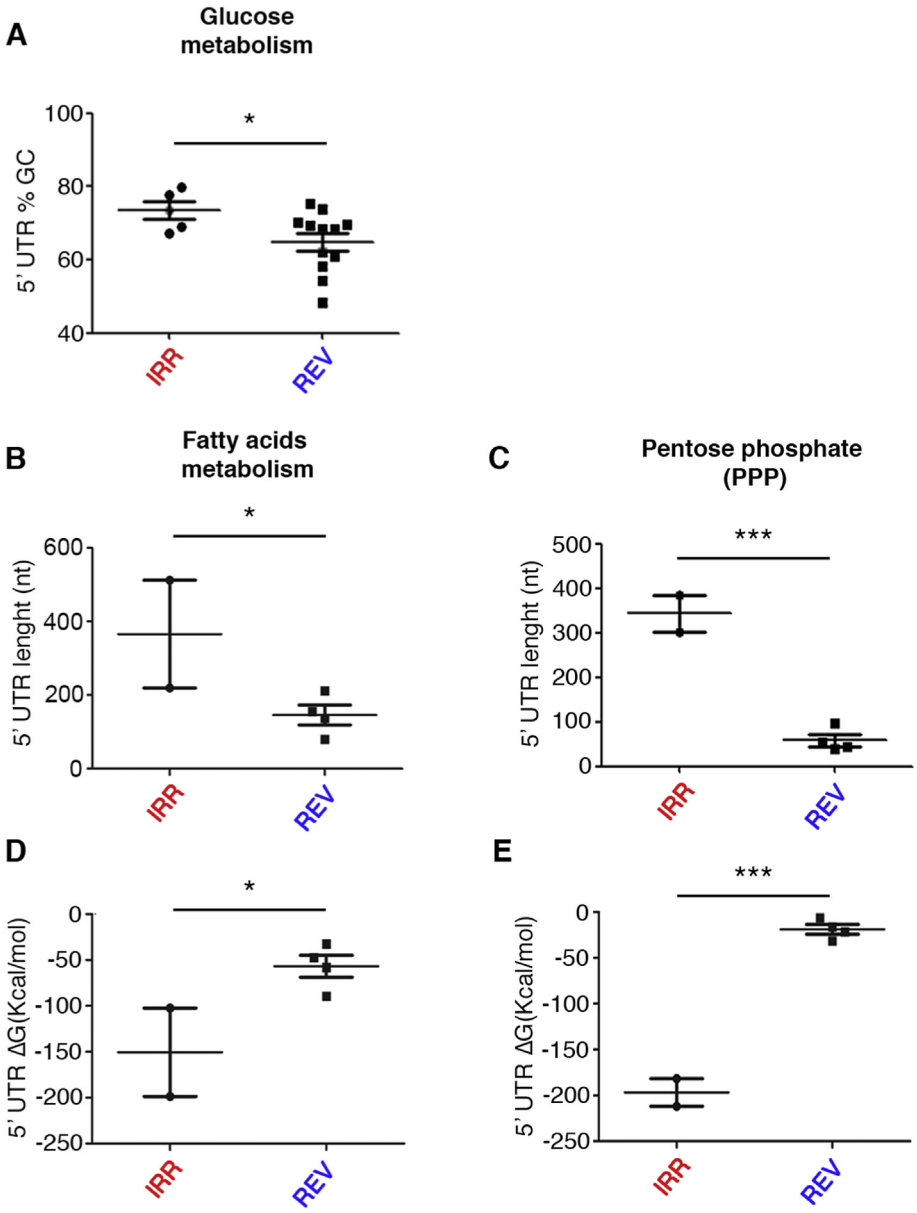

Fig. 6. mRNAs encoding for glycolytic enzymes possess GC-rich 5′UTRs while mRNAs encoding for enzymes involved in irreversible steps of the PPP and fatty acids synthesis possess very long and highly structured 5′UTRs.
(A) GC content of 5′UTRs of mRNAs encoding for enzymes involved in the metabolism of glucose. mRNAs were grouped in mRNAs encoding for enzymes involved in irreversible steps of glycolysis (IRR) and mRNAs encoding for enzymes involved in common glycolysis/gluconeogenesis steps (REV). (B) 5′ UTR length of mRNAs encoding for enzymes involved in the fatty acids metabolism. Fatty acids metabolism mRNAs were grouped in Fatty acids IRR (IRR), which encode for enzymes which catalyze irreversible steps of fatty acids synthesis and in Fatty acids REV (REV), which encode for enzymes that catalyze reversible steps of fatty acids metabolism. (C) 5′ UTR lenght of mRNAs encoding for enzymes involved in the pentose phosphate pathway (PPP). PPP mRNAs were grouped in PPP IRR (IRR), which encode for enzymes which catalyze irreversible steps of PPP and in PPP REV (REV), which encode for enzymes that catalyze reversible steps of PPP. (D) 5′ UTR ΔG of mRNAs encoding for enzymes involved fatty acids metabolism. PPP mRNAs were grouped in Fatty acids IRR (IRR), and in Fatty acids REV (REV), see Fig. 4C. (E) 5′ UTR ΔG of mRNAs encoding for enzymes involved in the pentose phosphate pathway (PPP). PPP mRNAs were grouped in PPP IRR (IRR), and in PPP REV (REV), see Fig. 4B. 5′UTR lenghts and ΔGs are indicated. Statistical *p*-values were calculated using unpaired one-tailed *t*-tests (NS: *p*-value > 0.05; *: *p*-value < 0.05).

limiting enzymes of fatty acid synthesis, such as ACACA and FASN, had the highest TEs (Fig. 3C). The pentose phosphate pathway (PPP) is an anabolic program essential for amino acid and nucleic acid production (Patra and Hay, 2014) (Waickman and Powell, 2012). When analyzing the TEs of PPP genes we found that also enzymes catalyzing for irreversible steps of the PPP showed the highest TEs among all PPP enzymes (Fig. 3D). Intriguingly the enzyme presenting the overall highest TE was RPIA (Fig. 3D and Supplementary File 1), which, although not being rate limiting, catalyzes the last fundamental step of the pathway, favouring conversion of Ribulose-5-phosphate to Ribose-5-phosphate, which is necessary for nucleic acids biosynthesis. Taken together, these results suggest that translational control acts on selected enzymes of the metabolic pathways that need to be switched on.

Next, we decided to independently test the efficacy and reliability of our ribosome profiling strategy. Through polysome profile fractioning followed by RT-qPCR, we validated the presence at the polysomes of a set of selected metabolic transcripts which we predicted to be translationally regulated (Fig. 4A). We found that the transcripts of glycolytic enzymes HK1 and PKM2 and of the fatty acids synthesis enzyme FASN were highly abundant in the polysome fractions of *in vitro* differentiated Th1 cells, in agreement with their predicted high TEs (Fig. 4B–D). We then checked if translation of such mRNAs was dependent on the mTORC1 pathway, which is fundamental for $CD4^+$ Th1 differentiation (Ray et al., 2015).We treated Th1 cells with Rapamycin, a well-known mTORC1 inhibitor, which affects translation of TOP mRNAs (Gismondi et al., 2014) and other eIF4F-dependent targets (Loreni et al., 2014). As expected, the TOP mRNA RPS29 was strongly removed from polysomes (Fig. 4E). A small but statistically significant effect was also seen for HK1, PKM2 and FASN mRNAs (Fig. 4B–D). *β-ACTIN* mRNA was insensitive to mTORC1 inhibition (Fig. 4F), as previously observed (Gorrini et al., 2005). Taken together these data confirm that HK1, PKM2 and FASN mRNAs are actively translated in human *in vitro* differentiated Th1 cells. Intriguingly, they seem to be only partially under the control of the mTORC1 signaling pathway, or, at least, less than TOP mRNAs.

Next, we wanted to understand whether the predictions of ribosome profiling data were also matched by protein levels. Our ribosome profiling data suggested that PKM2 (Dayton et al., 2016), necessary for the last irreversible step of glycolysis, i.e. pyruvate generation, was translationally regulated, whereas TPI1, that acts both in glycolysis and gluconeogenesis (Ationu et al., 1999), was regulated at the transcriptional level. We tested the mRNA and protein levels of PKM2 and TPI1

by performing western blots and RT-qPCRs on naïve $CD4^+$ T cells left untreated or polarized *in vitro* to Th1 for 7 days. Importantly, PKM2 had comparable mRNA levels in naïve and effector Th1 cells cells (Fig. 5A), but showed drastically increased protein amounts in $CD4^+$ differentiated Th1 cells by both fluorescence microscopy (Fig. 5B) and western blotting (Fig. 5 C). Conversely, TPI1 was highly regulated at the transcriptional level since both mRNA levels (Fig. 5D) and protein levels sharply increased in Th1 cells (Fig. 5E). These results are in agreement with ribosome profiling predicting no translational regulation. Thus, we conclude that translational regulation may primarily trigger the expression of enzymes involved in rate-limiting catabolic reactions of glucose metabolism, while the expression of enzymes involved in reversible steps of glycolysis may primarily be regulated at the transcriptional level.

Next, we focused on the PPP. By ribosome profiling, we predicted G6PD to be translationally regulated (Supplementary File 1). Indeed, we confirmed this scenario as we found highly increased protein levels of G6PD in Th1 differentiated $CD4^+$ T cells compared to naïve CD4 T cells, but only a slight but not significant increase of the corresponding mRNA (Fig. 5F and G).

3.3. Translational control may rely on specific 5′UTR features

Next, we attempted to understand the general mechanism of regulation by which enzymes involved in rate-limiting catabolic reactions are translationally regulated. The general mechanism is probably complex and may involve different types of regulatory elements. It is well-known that 5′ UTRs can adopt secondary and tertiary structures which affect proper initiation of translation of the downstream transcript (Leppek et al., 2018), therefore, we analyzed the 5′UTR sequence and structure of the most abundant transcript isoforms encoding for enzymes involved in glucose and fatty acids metabolism and in the PPP (Supplementary File 1). We found that the 5′UTR of mRNAs encoding for enzymes catalyzing irreversible steps of glycolysis were statistically more GC-rich (Fig. 6A) while transcripts encoding for enzymes catalyzing irreversible steps of either the PPP or fatty acids synthesis showed longer 5′ UTRs (Fig. 6B and 6C) with lower ΔG (Fig. 6D and E) (Supplementary File 1). We suggest that the complexity of the 5′UTR contributes to translational regulation, but does not fully explain the variety of regulations we found.

4. Discussion

Our study shows that translational control regulates the expression levels of specific metabolic enzymes in $CD4^+$ Th1 cells. Overall our study supports the model by which translation is not only coordinated with metabolism, but also acts upstream of metabolic steps, providing a feed-forward mechanism in which mitogenic and nutrient signaling activate a translational response (Biffo et al., 2018). Before discussing the biological implications of our findings, some technical caveats have to be briefly considered. In spite of several improvements, ribosome profiling requires a sufficient amount of actively translating cells. This requirement may be easily fulfilled in cell lines, but becomes a central issue when analyzing primary human cells. Specific care was taken in the continuous administration of cytokines and in the dilution of cells in order to avoid overcrowding effects. In spite of this, culturing conditions could be considered as a possible source of bias in the results we obtained. In addition, we were limited by the number of cells required for ribosome profiling, thus we had to focus on a single time point. Our study misses therefore transcriptional feedback loops that dynamically change the T cell response.

Another important issue is the *in vivo* relevance of the time course that we selected. Numerous lines of evidence have suggested that the generation of effector cells from a naive T cell takes several days, with T cell response typically peaking around 7–15 days after initial antigen stimulation (Kim et al., 2017). Most likely, our study reflects the late expansion phase of effector T cells and their polarization to the $Th1^+$ lineage (Geginat et al., 2014). The depth of our ribo-seq analysis, in spite of the high number of cells utilized, does not match that of other studies performed in cancer cells or in cell lines. Nonetheless, in our conditions, we can state that metabolism is regulated at the translational level in human effector T cells thanks to the relatively high abundance of metabolic mRNAs and the ease of their detection. However, we cannot exclude that other cellular processes, which rely on mRNAs that are near or below the detection threshold, may be equally regulated by translation. A simple model, driven by our data, is that transcriptional activity leads to the accumulation of some mRNAs, like PKM2 in our case, which are translationally silenced unless a specific pathway is activated. In this way, specific biochemical reactions are initiated only when multiple inputs are sensed by T cells.

Multiple pathways converge on the translational machinery (Roux and Topisirovic, 2018). It is expected that, in the conditions that we have run our analysis on, the main regulatory pathways acting on translation are all active. The mTORC1 pathway is essential for $Th1^+$ polarization (Ray et al., 2015). IFN-γ production requires the activity of Mnk1 (Salvador-Bernaldez et al., 2017), which is the kinase that, together with Mnk2, phosphorylates eIF4E (Ueda et al., 2004). PKC signaling, that is essential for the activation of eIF6 (Ceci et al., 2003; Miluzio et al., 2009, 2011, 2015), is well known to be important for all stages of T cell development (Baier and Wagner, 2009). Thus, the translational activity of $Th1^+$ cells may not be subset specific, but could simply reflect an efficient activation of the translational machinery by signaling pathways. If this were the case, we could expect that also other T cell subsets might behave similarly to Th1 cells for what concerns translational regulation of metabolism. This said, translation of transcripts harboring structured and/or GC-rich 5′UTRs is known to be highly affected by growth factors and overall translational rates (Brina et al., 2015; Roux and Topisirovic, 2018), i.e. the higher the translational rate the more efficiently the transcript is translated. Proliferation rates of different T cell subsets are quite different, implying that their translational rates could also differ. We thus can speculate that transcripts possessing a high TE in Th1 cells might not be so efficiently translated in other subsets with lower translational rates.

It was interesting to note that, in order to keep high levels of translation, we had to continuously supply cells with nutrients and dilute them. This observation raises the possibility that, *in vivo*, in the absence of nutrients and oxygen, tumor infiltrating lymphocytes, or more generally, infiltrating lymphocytes, rapidly adapt their secretory and metabolic profiles. Indeed, we expect that impaired translation leads to a cascade of events that changes the biological profile of cells without necessarily modifying the transcription level of certain mRNAs, such as PKM2. If this where the case, the development of technologies that score for the translational activity of single, infiltrating T cells would be largely required and highly informative.

In conclusion, we provide evidence for the translational regulation of specific metabolic enzymes in T cells. This regulation may consent T cells to adopt posttranscriptional modulation of metabolism pending microenvironmental clues that activate signaling cascades. Of these cascades, mTORC1 signalling is certainly important, but does not explain the whole complexity of translational regulation.

Author contributions

NM and SR designed the project, executed the experiments and analyzed the data. PC and AF performed experimental work and analyzed the data. RA and GV performed bioinformatic analyses. SB designed the experiments and analyzed data. NM and SB wrote the manuscript.

Funding

This work was supported by Europen Research Council (ERC) grant

TRANSLATE 338999 and AIRC Investigator Grant - IG 2017 to SB.

Data availability statement

The datasets generated for this study can be found in ArrayExpress under accession number E-MTAB-5961[1] (https://www.ebi.ac.uk/arrayexpress/experiments/E-MTAB-5961/) (Manfrini et al., 2019).

Declaration of competing interest

The authors declare that the research was conducted in the absence of any commercial or financial relationships that could be construed as a potential conflict of interest.

Acknowledgments

We would like to thank Dr. Nicholas T. Ingolia for his precious help and advice on ribosome profiling and Paola Gruarin for her help with Th1 differentiation.

Appendix A. Supplementary data

Supplementary data to this article can be found online at https://doi.org/10.1016/j.dci.2020.103697.

References

Ationu, A., Humphries, A., Lalloz, M.R., Arya, R., Wild, B., Warrilow, J., Morgan, J., Bellingham, A.J., Layton, D.M., 1999. Reversal of metabolic block in glycolysis by enzyme replacement in triosephosphate isomerase-deficient cells. Blood 94, 3193–3198.

Baier, G., Wagner, J., 2009. PKC inhibitors: potential in T cell-dependent immune diseases. Curr. Opin. Cell Biol. 21, 262–267.

Biffo, S., Manfrini, N., Ricciardi, S., 2018. Crosstalks between translation and metabolism in cancer. Curr. Opin. Genet. Dev. 48, 75–81.

Bonnal, R.J., Ranzani, V., Arrigoni, A., Curti, S., Panzeri, I., Gruarin, P., Abrignani, S., Rossetti, G., Pagani, M., 2015. De novo transcriptome profiling of highly purified human lymphocytes primary cells. Sci. Data 2, 150051.

Brina, D., Miluzio, A., Ricciardi, S., Clarke, K., Davidsen, P., Viero, G., Tebaldi, T., Offenhäuser, N., Rozmann, J., Rathkolb, B., Neschen, S., Klingenspor, M., Wolf, E., Gailus-Durner, V., Fuchs, H., Hrabe de Angelis, M., Quattrone, A., Falciani, F., S, B., 2015. eIF6 coordinates insulin sensitivity and lipid metabolism by coupling translation to transcription. Nat. Commun. 6, 8261.

Calamita, P., Miluzio, A., Russo, A., Pesce, E., Ricciardi, S., Khanim, F., Cheroni, C., Alfieri, R., Mancino, M., Gorrini, C., Rossetti, G., Peluso, I., Pagani, M., Medina, D.L., Rommens, J., Biffo, S., 2017. SBDS-deficient cells have an altered homeostatic equilibrium due to translational inefficiency which explains their reduced fitness and provides a logical framework for intervention. PLoS Genet. 13, e1006552.

Ceci, M., Gaviraghi, C., Gorrini, C., Sala, L.A., Offenhauser, N., Marchisio, P.C., Biffo, S., 2003. Release of eIF6 (p27BBP) from the 60S subunit allows 80S ribosome assembly. Nature 426, 579–584.

Dayton, T.L., Jacks, T., Vander Heiden, M.G., 2016. PKM2, cancer metabolism, and the road ahead. EMBO Rep. 17, 1721–1730.

Gallo, S., Ricciardi, S., Manfrini, N., Pesce, E., Oliveto, S., Calamita, P., Mancino, M., Maffioli, E., Moro, M., Crosti, M., Berno, V., Bombaci, M., Tedeschi, G., Biffo, S., 2018. RACK1 specifically regulates translation through its binding to ribosomes. Mol. Cell Biol. 38.

Gandin, V., Brina, D., Marchisio, P.C., Biffo, S., 2010. JNK inhibition arrests cotranslational degradation. Biochim. Biophys. Acta 1803, 826–831.

Gandin, V., Miluzio, A., Barbieri, A.M., Beugnet, A., Kiyokawa, H., Marchisio, P.C., Biffo, S., 2008. Eukaryotic initiation factor 6 is rate-limiting in translation, growth and transformation. Nature 455, 684–688.

Geginat, J., Paroni, M., Maglie, S., Alfen, J.S., Kastirr, I., Gruarin, P., De Simone, M., Pagani, M., Abrignani, S., 2014. Plasticity of human CD4 T cell subsets. Front. Immunol. 5, 630.

Gismondi, A., Caldarola, S., Lisi, G., Juli, G., Chellini, L., Iadevaia, V., Proud, C.G., Loreni, F., 2014. Ribosomal stress activates eEF2K-eEF2 pathway causing translation elongation inhibition and recruitment of terminal oligopyrimidine (TOP) mRNAs on polysomes. Nucleic Acids Res. 42, 12668–12680.

Gorrini, C., Loreni, F., Gandin, V., Sala, L.A., Sonenberg, N., Marchisio, P.C., Biffo, S., 2005. Fibronectin controls cap-dependent translation through beta1 integrin and eukaryotic initiation factors 4 and 2 coordinated pathways. Proc. Natl. Acad. Sci. U. S. A. 102, 9200–9205.

Hinnebusch, A.G., Ivanov, I.P., Sonenberg, N., 2016. Translational control by 5'-untranslated regions of eukaryotic mRNAs. Science 352, 1413–1416.

Hough, K.P., Chisolm, D.A., Weinmann, A.S., 2015. Transcriptional regulation of T cell metabolism. Mol. Immunol. 68, 520–526.

Ingolia, N.T., Brar, G.A., Rouskin, S., McGeachy, A.M., Weissman, J.S., 2012. The ribosome profiling strategy for monitoring translation in vivo by deep sequencing of ribosome-protected mRNA fragments. Nat. Protoc. 7, 1534–1550.

Ingolia, N.T., Lareau, L.F., Weissman, J.S., 2011. Ribosome profiling of mouse embryonic stem cells reveals the complexity and dynamics of mammalian proteomes. Cell 147, 789–802.

Jung, A.C., Paauw, D.S., 1998. Diagnosing HIV-related disease: using the CD4 count as a guide. J. Gen. Intern. Med. 13, 131–136.

Kim, C., Fang, F., Weyand, C.M., Goronzy, J.J., 2017. The life cycle of a T cell after vaccination - where does immune ageing strike? Clin. Exp. Immunol. 187, 71–81.

Lamming, D.W., Sabatini, D.M., 2013. A Central role for mTOR in lipid homeostasis. Cell Metabol. 18, 465–469.

Leppek, K., Das, R., Barna, M., 2018. Functional 5' UTR mRNA structures in eukaryotic translation regulation and how to find them. Nat. Rev. Mol. Cell Biol. 19, 158–174.

Lopez-Lluch, G., Hunt, N., Jones, B., Zhu, M., Jamieson, H., Hilmer, S., Cascajo, M.V., Allard, J., Ingram, D.K., Navas, P., de Cabo, R., 2006. Calorie restriction induces mitochondrial biogenesis and bioenergetic efficiency. Proc. Natl. Acad. Sci. U. S. A. 103, 1768–1773.

Loreni, F., Mancino, M., Biffo, S., 2014. Translation factors and ribosomal proteins control tumor onset and progression: how? Oncogene 33, 2145–2156.

Manfrini, N., Alfieri, R., Ricciardi, S., Biffo, S., 2019. Data from: Ribosome Profiling and RNA-Seq of in Vitro Differentiated Human CD4+ Th1 Cells. ArrayExpress.

Manfrini, N., Ricciardi, S., Miluzio, A., Fedeli, M., Scagliola, A., Gallo, S., Adler, T., Busch, D.H., Gailus-Durner, V., Fuchs, H., de Angelis, M.H., Biffo, S., 2017a. Data on the effects of eIF6 downmodulation on the proportions of innate and adaptive immune system cell subpopulations and on thymocyte maturation. Data Brief 14, 653–658.

Manfrini, N., Ricciardi, S., Miluzio, A., Fedeli, M., Scagliola, A., Gallo, S., Brina, D., Adler, T., Busch, D.H., Gailus-Durner, V., Fuchs, H., Hrabe de Angelis, M., Biffo, S., 2017b. High levels of eukaryotic Initiation Factor 6 (eIF6) are required for immune system homeostasis and for steering the glycolytic flux of TCR-stimulated CD4(+) T cells in both mice and humans. Dev. Comp. Immunol. 77, 69–76.

Michel, A.M., Ahern, A.M., Donohue, C.A., Baranov, P.V., 2015. GWIPS-viz as a tool for exploring ribosome profiling evidence supporting the synthesis of alternative proteoforms. Proteomics 15, 2410–2416.

Miluzio, A., Beugnet, A., Grosso, S., Brina, D., Mancino, M., Campaner, S., Amati, B., de Marco, A., Biffo, S., 2011. Impairment of cytoplasmic eIF6 activity restricts lymphomagenesis and tumor progression without affecting normal growth. Canc. Cell 19, 765–775.

Miluzio, A., Beugnet, A., Volta, V., Biffo, S., 2009. Eukaryotic initiation factor 6 mediates a continuum between 60S ribosome biogenesis and translation. EMBO Rep. 10, 459–465.

Miluzio, A., Oliveto, S., Pesce, E., Mutti, L., Murer, B., Grosso, S., Ricciardi, S., Brina, D., Biffo, S., 2015. Expression and activity of eIF6 trigger malignant pleural mesothelioma growth in vivo. Oncotarget 6, 37471–37485.

Miluzio, A., Ricciardi, S., Manfrini, N., Alfieri, R., Oliveto, S., Brina, D., Biffo, S., 2016. Translational control by mTOR-independent routes: how eIF6 organizes metabolism. Biochem. Soc. Trans. 44, 1667–1673.

Moore, M.J., Blachere, N.E., Fak, J.J., Park, C.Y., Sawicka, K., Parveen, S., Zucker-Scharff, I., Moltedo, B., Rudensky, A.Y., Darnell, R.B., 2018. ZFP36 RNA-binding proteins restrain T cell activation and anti-viral immunity. Elife 7.

Myers, D.R., Norlin, E., Vercoulen, Y., Roose, J.P., 2019. Active tonic mTORC1 signals shape baseline translation in naive T cells. Cell Rep. 27, 1858–1874 e1856.

Patra, K.C., Hay, N., 2014. The pentose phosphate pathway and cancer. Trends Biochem. Sci. 39, 347–354.

Peng, M., Yin, N., Chhangawala, S., Xu, K., Leslie, C.S., Li, M.O., 2016. Aerobic glycolysis promotes T helper 1 cell differentiation through an epigenetic mechanism. Science 354, 481–484.

Piccirillo, C.A., Bjur, E., Topisirovic, I., Sonenberg, N., Larsson, O., 2014. Translational control of immune responses: from transcripts to translatomes. Nat. Immunol. 15, 503–511.

Ray, J.P., Staron, M.M., Shyer, J.A., Ho, P.C., Marshall, H.D., Gray, S.M., Laidlaw, B.J., Araki, K., Ahmed, R., Kaech, S.M., Craft, J., 2015. The interleukin-2-mTORc1 kinase Axis defines the signaling, differentiation, and metabolism of T helper 1 and follicular B helper T cells. Immunity 43, 690–702.

Ricciardi, S., Manfrini, N., Alfieri, R., Calamita, P., Crosti, M.C., Gallo, S., Muller, R., Pagani, M., Abrignani, S., Biffo, S., 2018. The translational machinery of human CD4(+) T cells is poised for activation and controls the switch from quiescence to metabolic remodeling. Cell Metabol. 28, 895–906 e895.

Roux, P.P., Topisirovic, I., 2018. Signaling pathways involved in the regulation of mRNA translation. Mol. Cell Biol. 38.

Salvador-Bernaldez, M., Mateus, S.B., Del Barco Barrantes, I., Arthur, S.C., Martinez, A.C., Nebreda, A.R., Salvador, J.M., 2017. p38alpha regulates cytokine-induced IFNgamma secretion via the Mnk1/eIF4E pathway in Th1 cells. Immunol. Cell Biol. 95, 814–823.

Schwanhausser, B., Busse, D., Li, N., Dittmar, G., Schuchhardt, J., Wolf, J., Chen, W., Selbach, M., 2012. Global quantification of mammalian gene expression control. Nature 473, 337–342.

Truitt, M.L., Ruggero, D., 2016. New frontiers in translational control of the cancer genome. Nat. Rev. Canc. 16, 288–304.

Ueda, T., Watanabe-Fukunaga, R., Fukuyama, H., Nagata, S., Fukunaga, R., 2004. Mnk2 and Mnk1 are essential for constitutive and inducible phosphorylation of eukaryotic initiation factor 4E but not for cell growth or development. Mol. Cell Biol. 24, 6539–6549.

Waickman, A.T., Powell, J.D., 2012. mTOR, metabolism, and the regulation of T-cell differentiation and function. Immunol. Rev. 249, 43–58.

Zeng, H., Chi, H., 2017. mTOR signaling in the differentiation and function of regulatory and effector T cells. Curr. Opin. Immunol. 46, 103–111.